The following publication M. Muddassir, G. Limbert, B. Zhang, A. Duan, J. -J. Tan and D. Navarro-Alarcon, "Model Predictive Thermal Dose Control of a Robotic Laser System to Automate Skin Photorejuvenation," in IEEE/ASME Transactions on Mechatronics, vol. 28, no. 2, pp. 737-747, April 2023 is available at https://doi.org/10.1109/TMECH.2022.3218806.

Model Predictive Thermal Dose Control of a Robotic Laser System to Automate Skin Photorejuvenation

Muhammad Muddassir, *Student Member, IEEE*, Georges Limbert, Bin Zhang, Anqing Duan, Jun-Jong Tan and David Navarro-Alarcon, *Senior Member, IEEE*

***Abstract*—In this paper, we present a new method to control the thermal stimulation of skin during a photorejuvenation procedure. The proposed method can precisely administer the thermal dose while controlling the tissue's temperature under a safe limit. For that, a model-based treatment controller is developed and evaluated on a three-dimensional biophysics-based numerical model of skin; A hardware implementation is experimentally tested on a gelatin-based phantom tissue subjected to pulsed laser irradiation. A key component of our method is the use of a new thermal dose metric that enables quantifying and controlling the skin photo-rejuvenation process; This metric represents a suitable alternative to the lack of consensus on the metrics used by the photodermatology community. The reported experiments demonstrate that the developed controller endowed with the proposed dose unit can automatically deliver a prescribed laser irradiation and thermal dose over the tissue surface. The significance of our result is that it provides a control-theoretic framework to automate skin photorejuvenation treatments with thermal-guided robots. This approach has the potential to introduce standards in the automation of these types of photo-treatments.**

***Index Terms*—Robotics; Mechatronic systems; Model predictive control; Thermal imaging; Cosmetic dermatology.**

I. Introduction

TREATMENTS involving controlled heating of biological tissues are widely adopted in various medical disciplines. These thermal therapies can be divided into three categories according to the rate of temperature variation in the tissue [1], [2]. The first category is called hyperthermia treatment where the tissue's temperature rises to 41-44 °C in tens of minutes. This approach is typically used for destroying cancerous tumours which lie a few centimetres deep in the muscular tissue. Similarly, in cosmetic dermatology, treatments such as skin photorejuvenation, hair and tattoo removal, and lipolysis can be classified as hyperthermia treatments, where the superficial or hypodermal skin layers are targeted. Commonly-used heat sources in cosmetic dermatological treatments are high-intensity focused ultrasound (HIFU), microwaves, radio waves and laser light. The second category is coagulation treatment where the tissue's temperature rises to 50-100 °C in a few seconds. Examples of application include laser tissue welding and the destruction of warts and verrucas [3]–[5]. The last category is vaporisation treatment where the temperature of the tissue suddenly rises to 100 °C within one-tenth of a second. Applications of vaporisation include surgical incisions using lasers or electric arcs [6]–[8].

In most of clinical studies of hyperthermia, the amount of thermal stimulation or thermal dose are reported in cumulative equivalent minutes (CEM) at a treatment temperature of $T_t = 43°C$ [9]–[15]. Sapareto *et al.* [16] proposed the cumulative equivalent minutes (CEM) for quantifying the thermal dose administered in the tissue based on the exposure time at a treatment temperature of $43°C$. CEM is directly linked with the cytotoxic effect of heat where cell necrosis depends on the temperature and exposure time [16], [17]. CEM expresses the effect of various temperatures and exposure times in an equivalent exposure time in minutes at the treatment temperature of $43°C$. On the contrary, the dose in most photodermatological treatments is defined and prescribed in fluence (i.e., energy per unit of surface area, J/cm^2) or irradiance (i.e., power per unit of surface area, mW/cm^2) [18]. These units are more favourable for setting the parameters of a laser machine used in the treatments than providing any clinical insight.

In practice, the medical personnel can tune the power or exposure duration to administer the prescribed dose during the treatment. However, the thermal interaction between light and skin does not only depend on power or energy but also on the wavelength of the light and the structural composition of the skin. Considering that the characteristics of thermal stimulation are of prime importance during photorejuvenation, it is essential to define a treatment dose which considers both the temperature and the exposure time. Furthermore, exposing the tissue to a temperature of 41–$45°C$ for a few seconds is sufficient to achieve the optimal thermal stimulation (or thermal shock) [19], [20]. This optimal thermal stimulation enables the reconstruction and restructuring of the dermal collagen matrix, hence, improves the skin aesthetic condition [19]–[22]. Thus the need of defining a unit of photorejuvenation dose similar to hyperthermia seems more logical.

This work is supported in part by the Research Grants Council of Hong Kong under Grant 15212721, and in part by the Jiangsu Industrial Technology Research Institute Collaborative Funding Scheme under grant ZG9V. (Corresponding author: David Navarro-Alarcon).

Muhammad Muddassir, Bin Zhang, Anqing Duan, Jun-Jong Tan and David Navarro-Alarcon are with the Department of Mechanical Engineering, The Hong Kong Polytechnic University, Kowloon, Hong Kong. (e-mail: mohammad.muddassir@connect.polyu.hk, me-bin.zhang@connect.polyu.hk, aduan@polyu.edu.hk, junjongtan@aidlab.hk, dna@ieee.org)

G. Limbert is with the Department of Mechanical Engineering, Faculty of Engineering and Physical Sciences, University of Southampton, Southampton, UK and the Department of Human Biology, Faculty of Health Sciences, University of Cape Town, Observatory 7935, South Africa. (e-mail: g.limbert@soton.ac.uk)

In most settings for dermatology treatments, the pre/post temperature of the tissue is measured over a point at the surface of the skin. This approach is insufficient to monitor thermal propagation through the tissue and gain a full insight into the delivered thermal dose during the treatment. In our previous work [23], [24], we developed a robotic system capable of automatically performing skin photorejuvenation and reported a comparison study between the performance of this system and that of a human operator. Although the robot outperformed the practitioner in terms of accuracy and uniform distribution of the laser irradiation, it lacked the ability to monitor and control the thermal stimulation [23]. In order to address these limitations, in this work, we propose a new model predictive controller to achieve precise delivery of a target thermal dose onto the skin.

Many feedback controllers for maintaining the temperature of single points during hypothermia treatments have been reported in the literature [25]–[28]. These controllers typically require tuning several parameters that rely on prior knowledge of the model. Thus, a slight variation in parameters before or during treatment can compromise the stability of the controller. To monitor and control the tissue's temperature over a volume, researchers [29]–[33] used a rapidly switching focal array with magnetic resonance temperature imaging (MRTI) to heat a tumour while following a treatment path (such as spirals [29]–[31] or concentric circles [32], [33]). These controllers were only designed to monitor the temperature and could not simultaneously control the thermal dose. Arora *et al.* [34] proposed a thermal dose controller using a predictive model of a tumour, however, this model was restricted to one spatial dimension, which clearly limits its applicability. In summary, all aforementioned studies only addressed temperature elevation for treating cancer tumours. Also, they were designed to achieve high CEM values which require tens of minutes of thermal irradiation exposure.

In this paper, we are concerned with the problem of delivering a relatively small thermal dose to the surface of the skin while maintaining the temperature at $43°C$ to prevent coagulation. Controlling the thermal dose from temperature feedback is a complex control problem since the thermal dose and temperature are linked through a nonlinear relation. Due to the integral nature of this model and the thermal inertial-like effects, the dose in the tissue will keep accumulating at elevated temperatures, even if the input power is shut down. This temperature regulation problem is under-actuated, as the manipulated variables (input light profile at a single point) do not allow the control variable to maintain an arbitrary temperature profile in the tissue. To deal with these issues, in this work we develop a model-based thermal dose controller for predicting the effect of the thermal control actions and thus, administering the target thermal dose in the treated tissue. The novel contributions of this study are as follows:

1) Design of a model predictive controller (MPC) to deliver a target thermal dose D_f in the skin.
2) Definition of the prescribed dose for photorejuvenation in thermal dose unit for monitoring and controlling the thermal stimulation.
3) Design and development of a robotic platform for testing the performance of the thermal dose controller with a tissue phantom.
4) Evaluation of the performance of the proposed controller on an *in-silico* and gelatin-based tissue phantom; *in-silico* simulations are underpinned by a biophysics-based constitutive model of laser-skin photo-thermal interactions (see [35]).

To the best of the authors' knowledge, the proposed dose unit and thermal controller for photorejuvenation have never been reported in the literature. The motivation of our new method is conceptually depicted in Fig. 1. Table I presents the key nomenclature used throughout the paper.

The rest of the manuscript is organised as follows: Section II discusses the building blocks of the method. Section III elaborates on the controller design. Section IV evaluates the performance of the controller. Section V discusses the implications of methods and results. Section VI concludes the study.

TABLE I
KEY NOMENCLATURE

Symbol	Quantity
T	Tissue temperature at time t
T_t	Treatment temperature
T_r	Reference temperature
T_p	Predicted temperature for calculating $D_p(t)$
Q	Volumetric heat flux due to conduction
Q_b	Volumetric heat flux due to blood perfusion
Q_l	Volumetric heat flux due light-skin photothermal interaction
μ_a, μ_s	Absorption and scattering coefficient
Φ_a, Φ_s	Fluence rate due to absorption and scattering
$u(t)$	Pulse repetition rate
CES	Cumulative equivalent second
D_f	Target thermal dose
D	Thermal dose at time t
D_p	Potential thermal dose after $T > 39°C$

II. PHYSICS OF LASER-SKIN PHOTO-THERMAL INTERACTIONS

A. Constitutive Model

The thermal response of a homogeneous tissue is modelled using the Pennes' bioheat equation [36]:

$$\rho C \frac{\partial T(\mathbf{r},t)}{\partial t} = -\nabla Q(\mathbf{r},t) + Q_b(\mathbf{r},t) + Q_l(\mathbf{r},t). \quad (1)$$

where $\mathbf{r}$ is the position vector in Cartesian space $(x,y,z)^T$, ρ the density of the tissue $[kg/m^3]$ and C the specific heat capacity $[J/kg.°C]$. Q_b is computed by

$$Q_b = \omega_b C_b (T_a - T) \quad (2)$$

where T_a is the arterial blood temperature $[°C]$, ω_b the perfusion rate $[kg/m^3.s]$ and C_b the specific heat capacity of blood $[J/kg.°C]$.

B. Modelling Laser Light Distribution as a Control Input

The volumetric heat source Q_l due to laser-skin photo-thermal interaction in (1) is defined as [2], [35]:

$$Q_l(\mathbf{r},t) = \mu_a \Phi(\mathbf{r}) h(t). \quad (3)$$

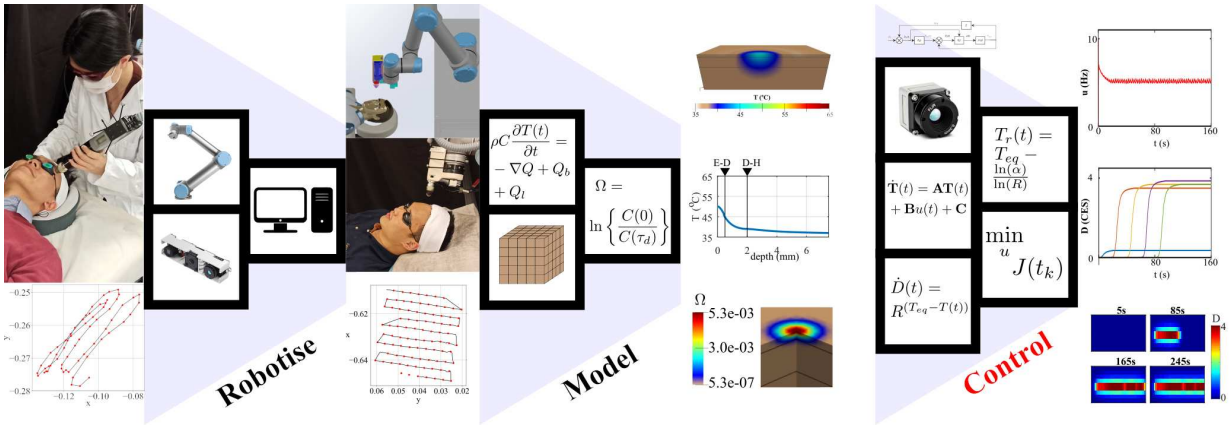

Fig. 1. Advancements in automated photorejuvenation treatment. From left to right, the conventional treatment was automated and robotised to improve the procedural efficiency [23], followed by the development of a simulation framework to study the thermal distribution in tissue, which can incorporate various biological, physical, and optical parameters of a tissue [35]. Quantification and control of the dose in photorejuvenation are presented here.

where μ_a denotes the light absorption coefficient of the tissue $[m^{-1}]$; $h(t)$ is a dimensionless time function which acts like a switch function to turn on/off the laser power; $\Phi(\mathbf{r})$ is the fluence rate of the irradiating light $[W/m^2]$ and conditions the distribution of heat generation in the tissue. Fig. 2(a) and (b) shows the distribution of fluence rate in the tissue along the x-axis and z-axis. $\Phi(\mathbf{r})$ is the sum of two fluence rate distributions, the fluence rate due to light absorption and that due to scattering, $\Phi(\mathbf{r}) = \Phi_a(\mathbf{r}) + \Phi_s(\mathbf{r})$. Φ_a is the fluence rate due to absorption and is modelled as [35]:

$$\Phi_a(\mathbf{r}) = (1 - r_{sp}) I_o I_r(x, y) I_b(z) \tag{4}$$

where r_{sp} is the specular reflection, I_o the incident light intensity $[W/m^2]$ and $I_r(x, y)$ the radial spread of light $[W/m^2]$ which follows a Gaussian profile [37]:

$$I_r(x, y) = \exp\big(-\{(x - x_o)^2 + (y - y_o^2)\}/W\big) \tag{5}$$

Here x_o and y_o are the coordinates of the centre of the laser beam in the xy-plane, and W is the width of the laser beam. $I_b(z) = (-\mu_a + (1 - g)\mu_s(z - z_o))$ is known as the Beer-Lambert law of coaxial attenuation. g and μ_s are the anisotropic factor and scattering coefficient $[m^{-1}]$, respectively.

The variable $h(t)$ represents a piecewise function that equals to 1 for the duration of a pulse width τ_p, otherwise equals to 0. In (1), $h(t)$ is a discontinuous variable that introduces heat into the tissues. To aid the design of the controller, we define the continuous control input $u(t)$ by assuming that the total power delivered during a pulse width τ_p is approximately equal to an average power over a period T_o:

$$\int_0^{T_o} \mu_a \Phi h(t) \mathrm{d}t \approx \int_0^{T_o} \mu_a \Phi \tau_p u(t) \mathrm{d}t \tag{6}$$

The control input $u(t)$ represents the frequency of the laser pulses, i.e., $u(t) = f_p = 1/T_o$. The assumption in (6) is analogous to that used in the calculation of the average power in a digital circuit when a power signal of pulse width modulation (PWM) shape is applied.

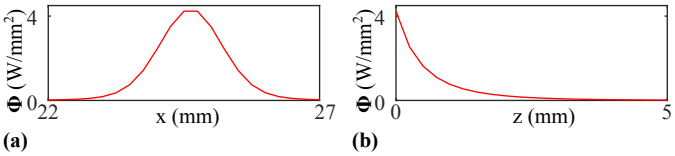

Fig. 2. Spatial distribution of the irradiated laser beam in the tissue. (a) Irradiation profile along x-axis. (b) Irradiation profile along z-axis. Φ represents the fluence and units are W/mm^2 and spatial units are mm

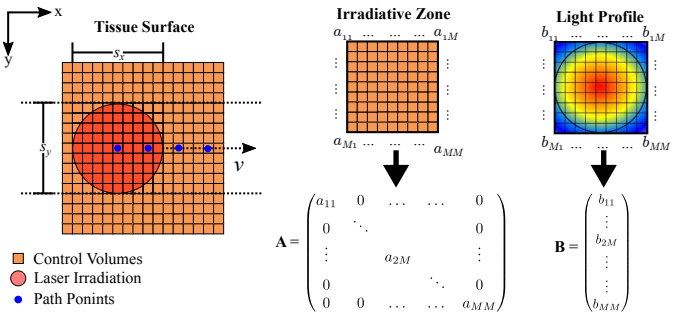

Fig. 3. Discretisation of the tissue into control volumes and construction of the matrics $\mathbf{A}$ and $\mathbf{B}$ in (7).

C. State-Space Formulation of Photo-Thermal Interaction

The spatio-temporal model of the thermal response in (1) can be approximated with a state-space model after spatial discretisation (as done, e.g., in Muddassir *et al.* [35]). This way, the system takes the following vector form:

$$\dot{\mathbf{T}}(t) = \mathbf{A}\mathbf{T}(t) + \mathbf{B}u(t) + \mathbf{C} \tag{7}$$

where $\mathbf{T}(t)$ is a vector containing the temperatures of N control volumes, $\mathbf{A} < 0 \in \mathbb{R}^{N \times N}$ is a diagonal matrix whose negative elements define the natural decay rate of the system, $\mathbf{B} \in \mathbb{R}^{N \times 1}$ is the input matrix computed via (3), and which maps the pulse rate input $u(t)$ into the temperature changes; The vector $\mathbf{C} \in \mathbb{R}^{N \times 1}$ defines the heat losses due to blood perfusion and heat conduction to neighbouring control volume. Figure 3 illustrates the constitution of the matrices $\mathbf{A}$ and $\mathbf{B}$ from the discretised tissue.

D. Thermal Dose

The thermal dose model by Sapareto *et al.* [16] is analogous to Arrhenius damage integral [38], which describes the protein inactivation rate at different temperature and time intervals. The thermal dose in Sapareto's method [16] calculates the equivalent time in minutes from the total exposure time at a temperature of $43°C$. This temperature value is set empirically based on the Arrhenius plot of the logarithm of the reciprocal versus the reciprocal of temperature [16], [39]–[42]. The exposure of tissue at treatment temperature T_t for a time duration Δt relates to an equivalent time Δt_{eq} as:

$$\Delta t_{eq} = \Delta t R^{(T_t - T(t))} \tag{8}$$

where $T(t)$ is the tissue temperature and T_t is the treatment temperature. Here, R is a dimensionless empirical parameter that depends on the tissue temperature [16]:

$$R = \begin{cases} 0.5 & T > 43°C \\ 0.25 & 39°C < T < 43°C \\ 0 & T < 39°C \end{cases} \tag{9}$$

The accumulated thermal dose is calculated by integrating the exposure time Δt whilst accounting for the tissue temperature. The deposited dose into the tissues (i.e., the CEM at $43°C$) is calculated as $D(t) = \int_0^{t_f} R^{(T_t - T(t))} \mathrm{d}t$.

The study presented in this paper focuses on skin photorejuvenation treatment, which requires the tissue temperature to be maintained at a treatment temperature for 4–8 seconds (s). This photo-thermal process stimulates collagen synthesis and remodelling in the epidermal and dermal tissue that enhances the aesthetic condition of the treated skin surface [19], [21], [22]. Therefore, we propose a smaller unit for photorejuvenation and named it *cumulative equivalent second* (CES), to properly adapt CEM in the photorejuvenation context. This metric is calculated as follows:

$$D(t) = \text{CES at } 43°C = \int_0^{t_f} R^{(T_t - T(t))} \mathrm{d}t \tag{10}$$

Maintaining the treatment temperature T_t for a duration of $\Delta t_{eq} = 4s$ implies the execution of four cumulative equivalent seconds. The concept of the thermal dose is found in the literature on hyperthermia treatments that cover a wide and diverse range of procedures. Generally, two types of units of thermal dose are used interchangeably in photodermatology: fluence (J/cm^2) and irradiance (mW/cm^2) [43]. However, these units lack specificity in terms of therapeutic actions. For example, if one irradiates a certain amount of fluence whilst using different wavelengths on biological tissues, each light wavelength exhibits a different thermal response. Tissues with specific optical properties—intrinsically linked to their microstructure and melanin content—irradiated with a fixed wavelength/fluence will exhibit different thermal responses.

Interactions of light and irradiated media highly depend on light wavelength and medium inter/intra-molecular structure; Fluence and irradiance might not be the most appropriate and objective quantities to serve as an input metric in phototherapies. On the other hand, CES depends on tissue temperature, which is a directly accessible physical quantity that can be measured by feedback sensors. Therefore, it is here proposed that CES is a more suitable unit for an automatic thermal control problem.

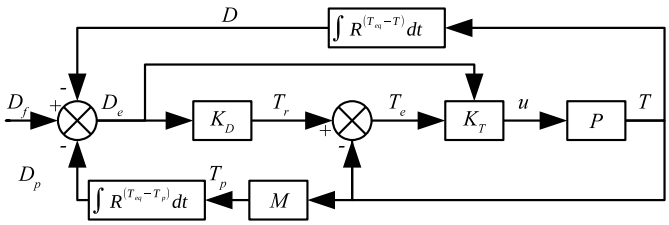

Fig. 4. Schematic diagram of thermal dose and temperature controller. P and M denote the phantom tissue and nominal model, respectively. D_e is the error between the final dose D_f and deposited plus potential dose $D + D_p$. T_e denotes the error between reference temperature T_r and current tissue temperature T.

III. Controller Design

A. Problem Statement

In this work, we aim to design an automatic set-point regulator that can administer a constant target dose D_f to each te spatial location inside the moving irradiative zone $[0 \leq x \leq s_x \ , \ 0 \leq y \leq s_y]$ in time t_f whilst prescribing the maximum allowable temperature and input frequency (pulse rate). In our method, we model the following temperature and input constraints:

$$\forall\ T(t) \in \mathcal{T} \ : \ \mathcal{T} = \{T \in \mathbb{R}; T \leq 43°C\} \tag{11}$$

$$\forall\ u(t) \in \mathcal{U} \ : \ \mathcal{U} = \{u \in \mathbb{R}; 0 \leq u \leq u_{max}\} \tag{12}$$

for u_{max} as the frequency upper limit imposed by the experimental hardware.

B. Controller Design

Commercially available cosmetic lasers for skin photorejuvenation offer relatively smaller laser beam diameters ranging from 1 to 20 mm, which limits their effective heating zone over the skin during treatment. During a treatment, the operator needs to manipulate the cosmetic laser in order to cover the treating area with laser irradiation. Here, we assume a similar scenario where a laser beam is moving with a constant speed $\|\mathbf{v}\|$ along a predefined path $\mathbf{P} = \{\mathbf{p}_1, \mathbf{p}_2, \ldots, \mathbf{p}_l\}$ composed of l points $\mathbf{p}_i$. The vector $\mathbf{v}$ represents the velocity of the computer-controlled laser.

Due to the motion of the laser and the limited surface coverage of irradiation, the controller must be able to increase the tissue temperature inside the irradiative zone in a given time duration t_f to deliver the target dose. The irradiative zone is modelled as a circumscribed square around the circular profile of the laser irradiation area, i.e., $s_x = s_y = d_l$, where d_l denotes the laser's diameter. t_f is a duration for which an observing location lies inside the irradiative zone, and is calculated from the laser diameter and the speed of the computer-controlled laser as $t_f = d_l / \|\mathbf{v}\|$.

Figure 4 shows the schematic diagram of the proposed control method. The thermal dose controller and temperature controller (which are respectively represented by the blocks

K_D and K_T) work in a master-slave configuration. The thermal dose controller K_D maps the error between the target D_f and the current dose $D(t)$ to the reference temperature $T_r(t)$. K_D is a feedback controller based on the inversion of the dose-temperature relationship which tunes the reference temperature $T_r(t)$ [44]. The temperature controller K_T helps to track $T_r(t)$ whilst constraining the thermal dose and temperature, and simultaneously considering hardware limitations.

In general, hyperthermia treatments last more than one hour or equivalently 30-45 CEM [16], [45]. In stark contrast to these durations, skin photorejuvenation procedures are conducted over shorter durations and require smaller thermal doses in the order of 4-8 CES. In the studies of Arora *et al.* [34], [44], [46], the lower rate of feedback for controlling the dose did not prevent the accurate delivery of the target dose. In these studies, the controller update time varied from tens of seconds to minutes. However, in the current study, the control problem pertains to photorejuvenation treatment which demands a faster controller response and smaller, but accurate, thermal dose deposition. Thus, the dose error $D_e(t)$ is fed to both controllers in order to prevent thermal overdosing.

C. Thermal Dose Controller K_D

The dynamic model of the thermal dose is derived from (10) and satisfies the following expression:

$$\dot{D}(t) = R^{(T_t - T(t))}. \tag{13}$$

The above relationship $M_1 : T \mapsto D$ maps the temperature $T(t)$ to the thermal dose $D(t)$ for a treatment temperature T_t. Therefore, for a given target dose D_f, there exists an inverse mapping $M_2 : D(t) \mapsto T_r(t)$, where the reference temperature $T_r(t)$ is calculated as:

$$T_r(t) = T_t - \frac{\ln(\alpha)}{\ln(R)} \tag{14}$$

for $\alpha = \frac{D_f - D(t)}{t_f - t}$ as the slope between the current dose and target dose D_f. t_f denotes the final time to deliver D_f and is a tunable parameter determining the responsivity rate of the controller. Here t_f is tuned according to the moving speed $\|\mathbf{v}\|$ of the laser and diameter of laser irradiation d_l. Since the laser source is moving at a constant speed, the controller has only $t_f = d_l/\|\mathbf{v}\|$ time to deliver the target dose. Note that the tuning of t_f under the above assumption will not always deliver the target dose, especially at a few starting locations in the path $\mathbf{P}$. The integrand in (10) depends on the error between the reference and current temperature and will yield a value greater than zero after $T(t) > 39°C$. Thus, the expression in (10) will increase after $39°C$ irrespective of the input power. This situation complicates the control of the thermal dose as the system's input $u(t)$ can only control the temperature increase; The cooling down of tissue depends on passive factors like convection and tissue's thermal properties. An estimate of the thermal dose from the current temperature can provide a better prediction of the required thermal dose. Thus, after $39°C$, there will be a potential thermal dose $D_p(t)$ which will be accrued without inputting any power. The accumulation of potential dose D_p depends on the decay rate of the dynamic system which is defined by $\mathbf{A}$. Before generating every control signal, $D(t)$ is calculated from (10) and $D_p(t)$ is estimated from the solution of the state space model in (7) as:

$$\mathbf{T}_p(t_c) = \mathbf{T}(t)e^{\mathbf{A}(t-t_c)} + \mathbf{A}^{-1}\mathbf{C}, \quad t_c \in [t, t + \Delta t_s] \tag{15}$$

where $\mathbf{T}_p(t)$ is the estimated temperature evolution that is used to compute the potential dose $D_p(t)$. Δt_s is the duration needed for the system to settle itself at $39°C$ and can be calculated as $\Delta t_s = \mathbf{A}^{-1}\ln(39/T(t)) - t$. At every time step, $\mathbf{T}_p(t)$ is estimated until the temperature drops to $39°C$ and the potential dose $D_p(t)$ is calculated based on the estimated values of $\mathbf{T}_p(t)$.

D. Temperature Controller K_T

A model predictive controller (MPC) is proposed to generate the control signal for controlling the tissue temperature (this controller is represented by the block K_T in Fig. 4). MPC can generate the control input whilst satisfying multiple physical/actuation constraints [47], which has shown as a promising tool for laser beam control [48] and thus makes it a suitable approach for our problem. At about 41-44$°C$, cell necrosis begins due to enzymatic alteration and activation. If the temperature continues to rise to $50°C$, irreversible cell necrosis may occur and the tissue undergoes a phase change similar to melting [2], also known as coagulation. Therefore, the controller must keep the tissue temperature under a safe limit when delivering the target dose.

To treat the tissue under strict constraints, we design a predictive model temperature controller K_T. The cost function in temperature controller K_T will ensure the deposition of the target dose D_f without violating biophysical, system and hardware constraints [49]. The optimisation problem is formulated as the minimisation the following cost, subject to various constraints:

$$\min_u J(t_k) = \sum_{i=1}^{p} w_D \left\{D_f - D(t_{k+i}) - D_p(t_{k+i})\right\}^2 + \sum_{i=1}^{p} w_T \left\{T_r(t_{k+i}) - T(t_{k+i})\right\}^2 + \sum_{j=1}^{m} w_u(t_j) \left\{u(t_{k+j-1})\right\}^2$$

$$\texttt{s.t.} \quad T(t_{k+i}) \leq T_t \tag{16}$$

$$D(t_{k+i}) \leq D_f \tag{17}$$

$$0 \leq u(t_{k+j}) \leq u_{max} \tag{18}$$

Here, p and m denote the prediction and control horizon, respectively. w_T and w_D are tunable parameters for penalising the cost function based on the errors in the temperature and dose, respectively. w_u is a penalty over the control effort, and u_{max} is the maximum rate of pulses of the laser. Qualitatively, to balance the competing objectives, higher priority calls for higher weight, which will result in smaller tracking error, and vice versa. Here the tasks of temperature and dose control are equally important, which implies that the same weights are assigned to these tasks, $w_D = w_T = 1$. As for control efforts penalization, we empirically set it to $w_u = 5$. Setting the w_u

greater than zero penalises the control input and avoids the overshooting of temperature.

This optimisation problem is solved iteratively in realtime using a numerical solver, the embedded conic solver ECOS [50], [51]. The optimisation problem seeks to find an optimal rate of laser irradiation which satisfies the system states and input constraints in (16), (17) and (18). After finding the optimal control sequence $u(t_{k+j})$, the first control action $u(t_0)$ of the sequence is applied to the plant system (i.e., either the phantom tissue P or the numerical simulation model M in Fig. 4) and a new temperature state will be obtained as the initial state of the next iteration. The values of $T(t_k)$ in the prediction horizon are estimated using (7). The model (13) estimates $D(t_k)$ in the prediction horizon.

IV. Results

A. Experimental Setup

Fig. 5 shows the experimental platform to evaluate the performance of the developed controller. The platform consists of a 2 DoF gantry robot, a thermal camera, a laser machine and a robot/laser controller. The gantry robot is a custom-built system that can move in two directions while holding the laser equipment vertically. The vertical orientation of the laser equipment ensures that the incident laser light irradiation is normal to the surface of the tissue phantom. For operating the robot within physical limits, IR distance sensors TOF10120 are embedded in the gantry structure. These sensors measure the distance with one-millimetre accuracy and have a data refresh rate of 10 Hz, which is sufficient to monitor the motion of the robot. A FLIR Boson thermal camera is attached to the robot's structure in a way that it can observe the tissue phantom without being occluded by the moving parts of the platform. This thermal camera has a frame rate of 60 Hz and captures images with a resolution of 320×240 and a measurement accuracy of $\pm 5\%\ ^\circ C$.

A gelatin-based tissue phantom is fabricated to mimic the optical [52] and thermal properties of human skin to physically test the robotic platform and its controller. The fabrication of the tissue consists of three steps: First, we dissolve 8 g gelatin, 0.35 g agar in 25 ml of water at $60^\circ C$ then add 0.05 g gouache brown colour to the mixture. The mixing of brown colour in the tissue phantom increases light absorption and gives the phantom a skin-like appearance. Then, we pour this solution into a $50\times50\times10mm^3$ cuboid mould. To remove any residual air, the solution is kept in a vacuum chamber for 30 min at $0.7atm$. Finally, the experiments are conducted after curing the tissue phantom in an airtight environment at $22^\circ C$ for 24 hours.

A Q-switched Nd:YAG 1064 nm laser is attached to the robot's end-effector to conduct the experiments. This type of laser is commonly used in a variety of dermatology treatments, including photoaging, rejuvenation, epilation, and removal of port-wine stain [53]. A short-pulsed 1064 nm laser light is used, whose energy is set to 0.75 J.

B. Parameter Identification

The negative matrix $\mathbf{A}$ in (7) defines the decay rate of the state variable $\mathbf{T}(t)$. It is assumed that the tissue phantom has a uniform decay rate throughout the surface. All diagonal values of $\mathbf{A}$ are equal, $\mathbf{A} = \beta\mathbf{I}$. To estimate $\beta < 0$, we irradiate the tissue phantom for 10 s, then let it thermally relax in order to decrease it to $39^\circ C$, as shown in Fig. 6(a). The temperature variations are recorded using the thermal camera and then filtered to identify the parameters of the exponential decay curve. The parameter identification is conducted by solving the following nonlinear optimisation problem:

$$\arg\min_{\alpha,\beta} \sum_i [T_i - (\alpha + e^{\beta t_i})]^2 \tag{19}$$

where T_i is the measured temperature values on each spatial location over time and α denotes the offset of the exponential distribution from the origin. Figure 6(b) shows the filtered temperature variations as a blue line which is used to estimate the exponential parameters. The dotted line is an exponential function whose parameters are estimated from fitting.

The thermal response of the phantom tissue due to laser irradiation is identified using the instantaneous temperature change upon irradiation. Since the fabricated tissue phantom has low thermal conductivity, the instantaneous conduction and perfusion in the tissue at t^+ after irradiation at t is approximately zero, i.e., $\nabla Q \approx 0$ and $Q_b \approx 0$. Then (1) simplifies to:

$$\rho C \frac{\partial T(t)}{\partial t} = Q_l \tag{20}$$

Figure 7(a) shows the thermal distribution on the surface of the tissue phantom at t^+. Figure 7(b) illustrates the filtered temperature values along the horizontal x-axis and the estimated profile of the power deposition, which follows Gaussian distribution. Three parameters define this type of distribution: mean, standard deviation and amplitude. The amplitude of the Gaussian distribution is identified using (20). The mean and standard deviation is the physical location and beam diameter of the irradiating laser, respectively.

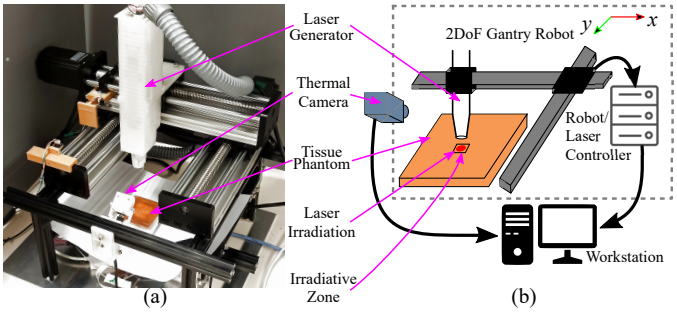

Fig. 5. Experimental Setup. (a) Developed experimental setup and gelatin-based tissue phantom. (b) Schematic diagram of the experimental setup highlighting the connections between each of its component.

C. Controlled Thermal Stimulation

The performance of the developed controller is evaluated on an *in-silico* simulation platform and a physical experimental platform. For the experiments reported in Fig. 10 and Fig. 11, the laser energy is set to $0.75J$ and the diameter of the laser beam is set to $2mm$. The horizontal and vertical dimensions of the irradiative zone are limited to $3mm$ in both simulations and

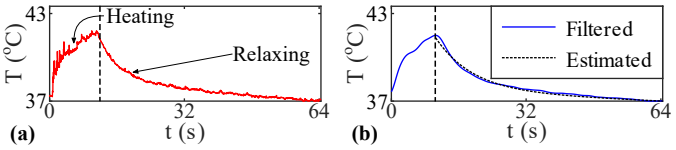

Fig. 6. Parameter identification of the decaying coefficient β. (a) Temperature evolution during the heating and relaxing phase of tissue. (b) The filtered temperature measurements are plotted in blue colour and the dotted curve is the fitted curve after estimating the exponential curve parameters.

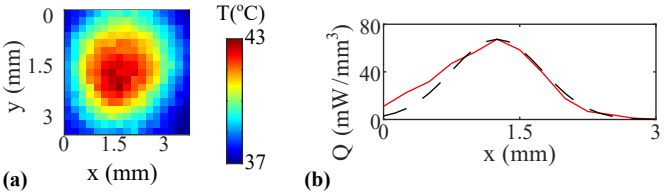

Fig. 7. Parameter identification of the power deposition Q_l. (a) Temperature distribution on the tissue surface upon irradiation. (b) Calculated and estimated profile of the power deposition.

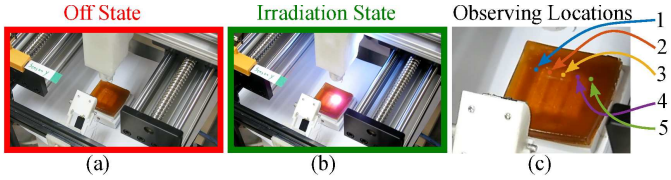

Fig. 8. Physical setup during experiments. The laser generator is moving over tissue phantom during experiments: (a) show the off laser state and (b) the on laser state. (c) The observing location on the tissue phantom. The data for these location are plotted in Fig. 10, 11, and 12.

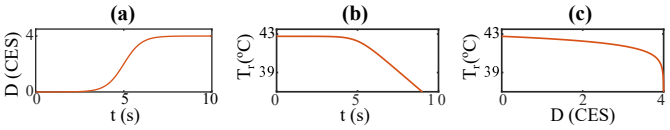

Fig. 9. Response of the thermal dose controller based on dose deposition. (a) Thermal dose with respect to time. (b) Reference temperature $T_r(t)$ dose profile in (a). (c) Response of the thermal dose controller K_D from initial to final dose.

physical experiments. In the MPC, the prediction and control horizons are set to $2s$ thus $p = m = 20$ as time step was $\Delta t = 0.1s$. For the experiments shown in Fig. 10 and Fig. 11, t_f is set to $10s$ and $5.55s$ according to the velocities of the laser source which are $0.1mm/s$ and $0.18mm/s$, respectively. The maximum pulse repetition rate is set to $u_{max} = 10Hz$ in (18), whereas maximum allowable temperature and target thermal dose are $T_t = 43°C$ and $D_f = 4CES$, respectively. In the simulated tissue phantom, the effect of blood perfusion is not considered in order to imitate the physical composition of the gelatin-based tissue phantom.

All the experimental results are reported in a similar format including identical scales for convenient comparison in Fig. 10, Fig. 11, and Fig. 12. The first row in the figures shows the pulse rate (frequency) of the laser irradiation which is generated by the temperature controller K_T. The second row contains the temperature evolution at various spatial locations with respect to time and the third row depicts the deposition of thermal dose in these locations with respect to time. The fourth and fifth rows illustrate the temperature and thermal dose distribution over the observed surface of the tissue for various time steps. For all simulations and physical testing, the laser beam was moving $5cm$ from the left to right boundary of the tissue.

Initially, the temperature of the tissue phantom is $37°C$ and the thermal dose deposition is zero CES. Figure 9 (a) shows a dose deposition profile and Fig. 9 (b) illustrates the reference temperatures generated by the thermal dose controller K_D based on this dose profile. The thermal dose controller K_D set the reference temperature $T_r(t)$ at maximum allowable temperature $(43°C)$ to steer the tissue temperature to the reference temperature in minimum time t_f, which forced the temperature controller K_T to generate the maximum pulse repetition rate for steering the tissue temperature to the reference temperature. When the tissue temperature approaches the reference temperature, the deposition of the thermal dose starts to increase, which decreases the error between the current and target thermal dose. This signals the thermal dose controller K_D to set a lower reference temperature. Then, temperature controller K_T compensates for the change in the reference temperature and lowers the pulse repetition rate. That aids the controller to decrease the rate of thermal dose deposition in order to achieve the target thermal dose without violating the temperature or dose constraints.

In Fig. 10(a), the sudden dips of controller outputs are due to the impulsive nature of the hardware that irradiates the laser light in pulse mode. As setting any frequency greater than zero will force the laser control system to irradiate, which could further increase the temperature and then lead to the violation of temperature or dose constraints at that instance. This behaviour of the controller is more apparent when performing the experiments with a lower speed of the laser source, as shown in Fig. 10(a). Figures 10(f)–(j) show the controller's output and thermal response of the experiment with simulated tissue phantom and the laser source moves at $0.18mm/s$.

The performance of the developed controller is also evaluated on the physical gelatin-based tissue phantom. The experiments are performed on the developed platform, as shown in Fig. 5. Figure 11 shows the controller output and the thermal response of the tissue phantom during laser irradiation. In Fig. 11, the trends of the temperature evolution and dose deposition are similar to those of the numerical simulation. However, the resulting temperature and dose distributions over the surface look more diffused than in Fig. 10(d), (e), (i) and (j). One possible reason for the differences is that the water in the actual tissue phantom increases its thermal conductivity.

D. Unrealisable Control

The proposed controller can administer a target dose on the predefined path without violating the constraints in previous experiments. The initial assumptions of keeping the displacement speed of the laser source and energy of the laser beam constant simplify the control design and its implementation. However, this approach has limited capability to administer

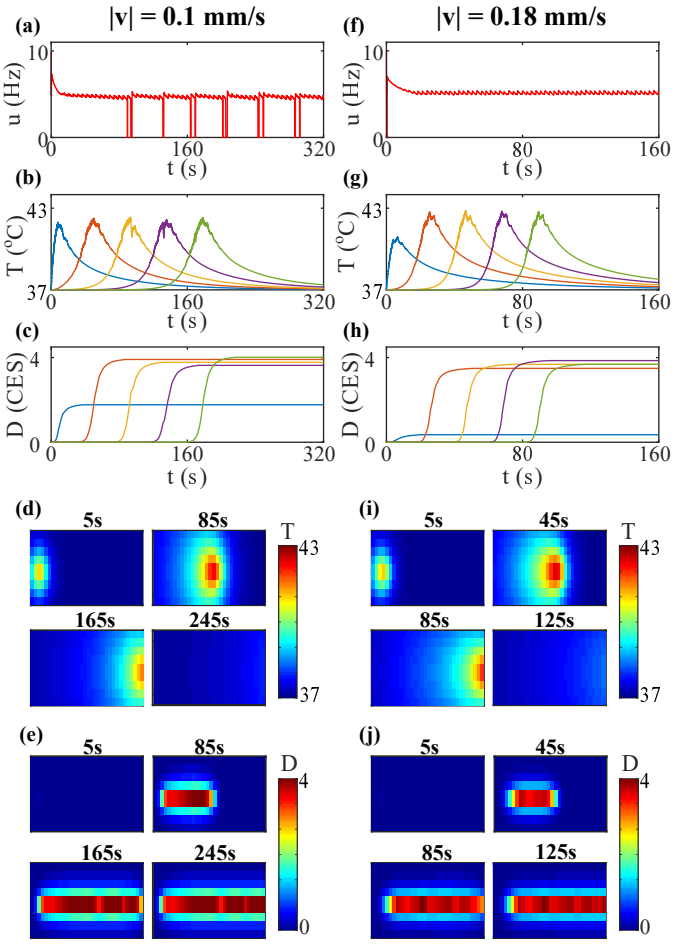

Fig. 10. Simulation results. Treating the simulated tissue phantom when the displacement speed of the laser beam is $0.1mm/s$ and $0.18mm/s$. For both cases, the laser energy was $0.75J$, laser beam diameter is $2mm$ and $p = m = 20$. (a) and (f) are the control signal generated by the developed controller. (b) and (g) are the temperature of various points on the surface which are $3mm$ apart from each other. (c) and (h) are the dose deposition on each monitored surface point. (d) and (i) show the temperature distribution on the treated surface at four time instances. The size of the shown surface is $4 \times 15mm^2$. (d) and (i) show the thermal dose distribution on the treated surface at four time instances. The size of the shown surface is $4 \times 15mm^2$.

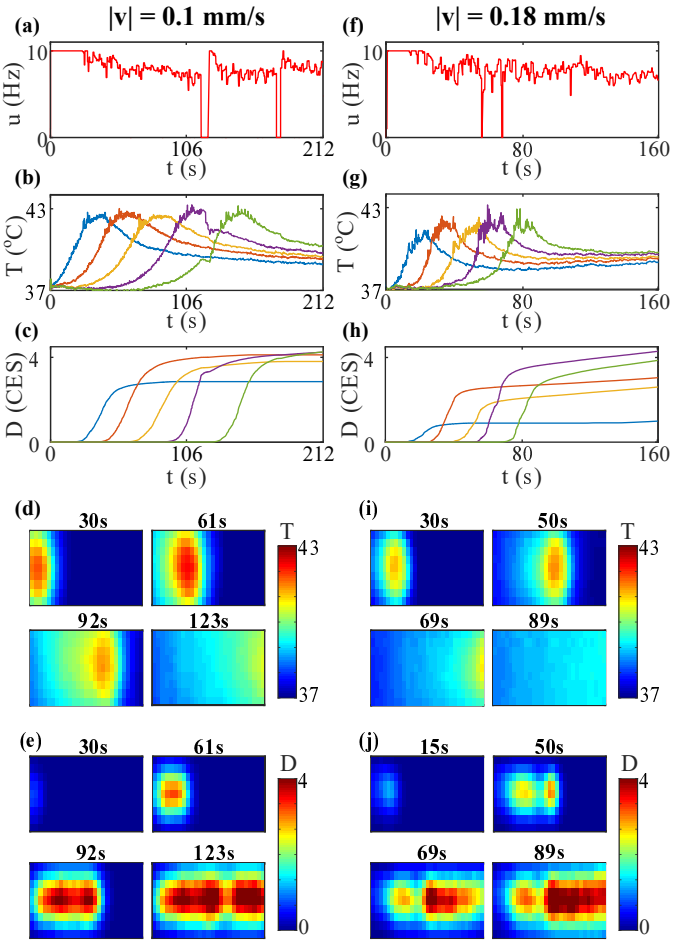

Fig. 11. Experimental results. Treating the gelatin-based tissue phantom when the displacement speed of the laser beam is $0.1mm/s$ and $0.18mm/s$. For both cases, the laser energy was $0.75J$, the laser beam diameter is $2mm$ and $p = m = 20$. (a) and (f) are the control signal generated by the developed controller. (b) and (g) are the temperature of various points on the surface which are $3mm$ apart from each other. (c) and (h) are the dose deposition on each monitored surface point. (d) and (i) show the temperature distribution on the treated surface at four time instances. The size of the shown surface is $4 \times 15mm^2$. (d) and (i) show the thermal dose distribution on the treated surface at four time instances. The size of the shown surface is $4 \times 15mm^2$.

a larger thermal dose or at higher velocities of the laser source. In Fig. 12, two experiments are presented where the control method is no longer able to deliver the target dose. The experiment shown in Figs. 12(a)–(e), the energy of the laser pulse is set to $0.5J$ and speed is set to $0.18mm/s$. The controller is continuously generating a control signal near the maximum pulse rate but the system is not able to approach the target state in the final time t_f, which shows that a realisable control cannot be guaranteed within this range of parameters. The same outcome is observed when the speed of the laser source is set to $0.376mm/s$, as shown in Fig. 12(f)–(j). The control signal is close to the maximum pulse rate but the target dose can not be administered. The accompanying multimedia video demonstrates the conducted experiments.

V. Discussion

This study proposes, develops, and implements a method to optimise thermal stimulation for automated photorejuvenation treatments. Conventionally, the treatment dose in skin photorejuvenation is prescribed and administered in irradiance (mW/cm^2) or fluence (J/cm^2). Although these units are helpful for a practitioner to accurately set the laser machine before treatment, they are insufficient to predict and control the target dose. Typically, the thermal response of tissue under irradiation depends on various factors, e.g., light wavelength, the physical properties and structural composition of the irradiated material, and the mode of irradiation (pulse or continuous). As a result, real-time dose delivery cannot be measured during treatment and it can only be assessed posteriorly using visual inspection or specialised image processing software/hardware in current clinical settings. In view of this, this paper proposes to modify the thermal dose calculation, resulting in a cumulative equivalent second, for real-time quantification of the thermal response by irradiating light, which finds its origin in hyperthermia treatment. Considering the thermal dose in this context provides an achievable target to track and aids in

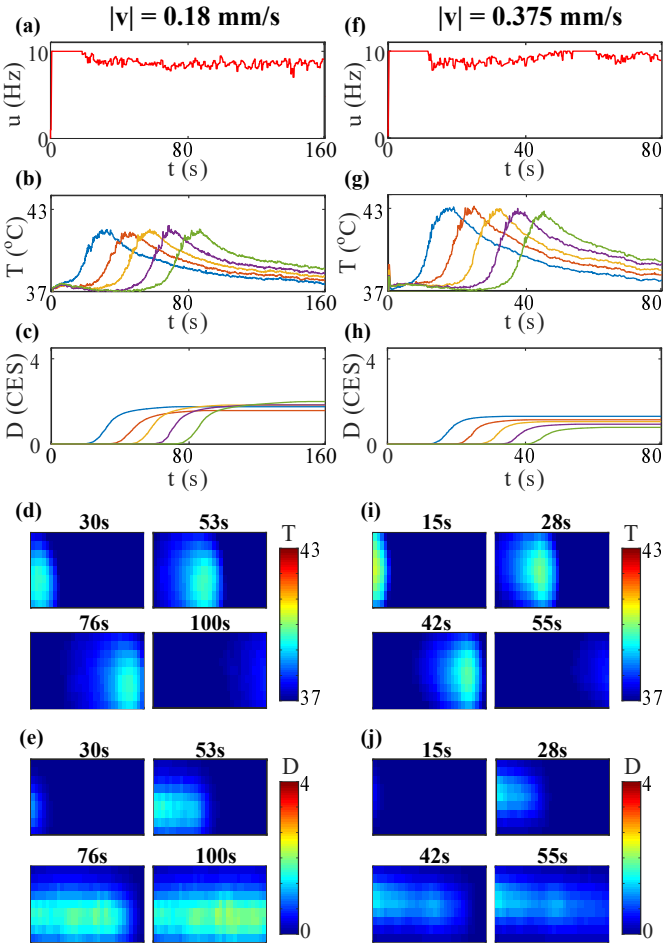

Fig. 12. Experimental results. Treating the treated gelatin-based tissue phantom when the displacement speed of the laser beam is $0.18mm/s$ and $0.375mm/s$. The laser energy is $0.5J$ and $0.75J$ for the first and second case respectively, laser beam diameter was $2mm$ and $m = p = 20$. (a) and (f) are the control signal generated by the developed controller. (b) and (g) are the temperature of various points on the surface which are $3mm$ apart from each other. (c) and (h) are the dose deposition on each monitored surface point. (d) and (i) show the temperature distribution on the treated surface at four time instances. The size of the shown surface is $4 \times 15mm^2$. (d) and (i) show the thermal dose distribution on the treated surface at four time instances. The size of the shown surface is $4 \times 15mm^2$.

formulating a solvable control problem, the control stimulation from the proposed control problem can be achieved by developing a thermal dose and temperature controller, which works in a master-slave configuration. More precisely, the dose controller generates a reference temperature trajectory and a model predictive temperature controller efficiently follows the reference temperature while satisfying the states, inputs and hardware constraints.

The developed control strategy is tested with both *in-silico* and gelatin-based tissue phantom. The physical parameters are kept similar while experimenting on both platforms. To minimise the effect of plant-model mismatch and to optimise the performance of the controller, parameter identification is performed before the experiments. Subsequently, these parameters are used in both numerical simulation and physical experiments. The control signal regulates the number of light pulses per second with a laser source irradiating the pulses. The experimental results demonstrate that the thermal dose on the observed locations on the surface is approaching the target dose D_f within time t_f. The surfaces with coloured-valued in Fig. 10 and 11 show the dose deposition on the treated area at various time points. Notably, the responsiveness of the controller is exhibited by the sudden dips in the control signal, as the controller can suddenly invoke the lowest input value to avoid the violation of state constraints.

Still, there are a few limitations that shall be mentioned. When considering real skin, there is a large number of physical and biological factors with inherent variability which could affect the controller performance. For example, relative humidity, thermal convection, and noisy measurements can directly degrade measurement quality in control methods. Besides, the water and oil content on the skin surface, skin tone (i.e. melanin concentration), blood perfusion rate, and thickness of skin are highly variable among different individuals and are also variable within the same individual due to age, health status or environmental conditions [54], [55]. In addition, the current simulation environment does not consider the variations in water content and volume of the tissue due to temperature variations.

For future work, we would like to establish a more detailed tissue model in order to improve the accuracy of the estimated temperature distribution in the simulation environment. To completely automate the controlled thermal stimulation, an advanced controller will have to be designed such that the motion commands can be generated while delivering a uniform thermal dose over a given skin surface. It is also interesting to introduce multi-modality thermal sensors to monitor temperature [56], which is likely to be a viable option to improve reliability and uncertainty estimation/control.

VI. Conclusion

In this work, we have proposed a control method to thermally stimulate the skin in photorejuvenation. It consists of a thermal dose and temperature controller in a master-slave configuration, where the inverse model of the thermal dose controller sets the reference temperature for a model predictive temperature controller. The temperature controller generates the rate of laser pulses that enforces the system to reach a reference temperature over the surface. Key to this goal is the introduction of a modified unit of thermal dose that enables to quantify, monitor and servo-control the thermal stimulation process. This approach was implemented on an *in-silico* and a physical platform to validate the performance with numerical models and phantom tissues, respectively. The proposed new methodology provides an intuitive control-theoretic framework for automating thermal skin stimulation in other dermatological treatments, such as hair and tattoo removal. Future work includes the incorporation of other parameters of the moving laser source like displacement, speed and energy, into the controller's formulation. Also, our team is currently working on the implementation of this new approach in an automatic face rejuvenation system (see [23]); Tests with human subjects will be conducted to compare the method's aesthetic outcome with the current manual practice. This control strategy can

be conveniently adapted for a 3D curved surfaces, if the irradiative zone is kept relatively smaller. As the input to the control method is temperature values of irradiative zone instead of the temperatures of a whole surface.

REFERENCES

[1] F. Xu and T. Lu, "Skin bioheat transfer and skin thermal damage," in *Introduction to Skin Biothermomechanics and Thermal Pain*. Springer Berlin Heidelberg, 2011, pp. 23–86.

[2] F. Xu, T. J. Lu, K. A. Seffen, and E. Y. Ng, "Mathematical modeling of skin bioheat transfer," *Appl. Mech. Rev.*, vol. 62, no. 5, pp. 1–35, 2009.

[3] Y. Mistry, S. Natarajan, and S. Ahuja, "Evaluation of laser tissue welding and laser-tissue soldering for mucosal and vascular repair," *Annals of Maxillofacial Surgery*, vol. 8, no. 1, p. 35, 2018.

[4] L. S. Bass and M. R. Treat, "Laser tissue welding: A comprehensive review of current and future," *Lasers Surg. Med.*, vol. 17, no. 4, pp. 315–349, 1995.

[5] H. zgr and A. Grkan, "Therapeutic Lasers and Skin Welding Applications," in *A Roadmap of Biomedical Engineers and Milestones*, S. Kara, Ed. InTech, June 2012.

[6] A. Martens, K. Pader, T. Prange, K. F. Ortved, and D. W. Richardson, "Minimally Invasive Surgical Techniques," in *Equine Surgery*. Elsevier, 2019, pp. 214–233.

[7] D. W. Scott and W. H. Miller, "Dermatologic Therapy," in *Equine Dermatology*. Elsevier, 2011, pp. 101–129.

[8] S. Grimnes and O. G. Martinsen, "Selected Applications," in *Bioimpedance and Bioelectricity Basics*. Elsevier, 2015, pp. 405–494.

[9] E. L. Jones, J. R. Oleson, L. R. Prosnitz, T. V. Samulski, Z. Vujaskovic, D. Yu, L. L. Sanders, and M. W. Dewhirst, "Randomized Trial of Hyperthermia and Radiation for Superficial Tumors," *J. Clin. Oncol.*, vol. 23, no. 13, pp. 3079–3085, May 2005.

[10] M. Franckena, D. Fatehi, M. d. Bruijne, R. A. Canters, Y. v. Norden, J. W. Mens, G. C. v. Rhoon, and J. v. d. Zee, "Hyperthermia dose-effect relationship in 420 patients with cervical cancer treated with combined radiotherapy and hyperthermia," *Eur. J. Cancer*, vol. 45, no. 11, pp. 1969–1978, July 2009.

[11] D. S. Kapp and R. S. Cox, "Thermal treatment parameters are most predictive of outcome in patients with single tumor nodules per treatment field in recurrent adenocarcinoma of the breast," *InterNatl. J. (Wash.) of Radiation Oncology Biology Physics*, vol. 33, no. 4, pp. 887–899, 1995.

[12] J. R. Oleson, T. V. Samulski, K. A. Leopold, S. T. Clegg, M. W. Dewhirst, R. K. Dodge, and S. L. George, "Sensitivity of hyperthermia trial outcomes to temperature and time: Implications for thermal goals of treatment," *InterNatl. J. (Wash.) of Radiation Oncology Biology Physics*, vol. 25, no. 2, pp. 289–297, Jan. 1993.

[13] M. Sherar, F.-F. Liu, M. Pintilie, W. Levin, J. Hunt, R. Hill, J. Hand, C. Vernon, G. van Rhoon, J. van der Zee, D. G. Gonzalez, J. v. Dijk, J. Whaley, and D. Machin, "Relationship between thermal dose and outcome in thermoradiotherapy treatments for superficial recurrences of breast cancer: Data from a phase III trial," *InterNatl. J. (Wash.) of Radiation Oncology Biology Physics*, vol. 39, no. 2, pp. 371–380, 1997.

[14] R. D. Issels, S. W. Prenninger, A. Nagele, E. Boehm, H. Sauer, K. W. Jauch, H. Denecke, H. Berger, K. Peter, and W. Wilmanns, "Ifosfamide plus etoposide combined with regional hyperthermia in patients with locally advanced sarcomas: a phase II study." *J. Clin. Oncol.*, vol. 8, no. 11, pp. 1818–1829, Nov. 1990.

[15] B. Rau, P. Wust, W. Tilly, J. Gellermann, C. Harder, H. Riess, V. Budach, R. Felix, and P. Schlag, "Preoperative radiochemotherapy in locally advanced or recurrent rectal cancer: regional radiofrequency hyperthermia correlates with clinical parameters," *InterNatl. J. (Wash.) of Radiation Oncology Biology Physics*, vol. 48, no. 2, pp. 381–391, Sept. 2000.

[16] S. A. Sapareto and W. C. Dewey, "Thermal dose determination in cancer therapy," *InterNatl. J. (Wash.) of Radiation Oncology, Biology, Physics*, vol. 10, no. 6, pp. 787–800, 1984.

[17] G. C. Van Rhoon, "Is CEM43 still a relevant thermal dose parameter for hyperthermia treatment monitoring?" *Int. J. Hyperth.*, vol. 32, no. 1, pp. 50–62, 2016.

[18] H. Lui and R. R. Anderson, "Radiation sources and interaction with skin," in *Photodermatology*, H. W. Lim, H. Hönigsmann, and J. L. M. Hawk, Eds. CRC Press, feb 2007, pp. 29–40.

[19] S. D. Dams, M. de Liefde-van Beest, A. M. Nuijs, C. W. Oomens, and F. P. Baaijens, "Pulsed heat shocks enhance procollagen type I and procollagen type III expression in human dermal fibroblasts," *Skin Res. Tech.*, vol. 16, no. 3, pp. 354–364, 2010.

[20] R. A. Weiss, D. H. McDaniel, and R. G. Geronemus, "Review of nonablative photorejuvenation: Reversal of the aging effects of the sun and environmental damage using laser and light sources," *Semin. Cutan. Med. Surg.*, vol. 22, no. 2, pp. 93–106, June 2003.

[21] S. Dams, "The effect of heat shocks in skin rejuvenation," *Universiteitsdrukkerij TU Eindhoven, The Netherlands ©Koninklijke*, no. 2010, p. 129, 2010.

[22] S. D. Dams, M. De Liefde-van Beest, A. M. Nuijs, C. W. Oomens, and F. P. Baaijens, "Heat shocks enhance procollagen type I and III expression in fibroblasts in ex vivo human skin," *Skin Res. Tech.*, vol. 17, no. 2, pp. 167–180, 2011.

[23] M. Muddassir, D. Gomez Dominguez, L. Hu, S. Chen, and D. Navarro-Alarcon, "Robotics meets cosmetic dermatology: Development of a novel vision-guided system for skin photo-rejuvenation," *IEEE/ASME Trans Mechatronics*, vol. 27, no. 2, pp. 666–677, April 2022.

[24] M. Muddassir, S. U. Chan, D. Gomez, and D. Navarro-Alarcon, "Can a robot outperform a human operator in skin photorejuvenation?" *J. Cosmet. Dermatol.*, vol. 1, no. February, pp. 1–2, 2021.

[25] P. VanBaren and E. Ebbini, "Multipoint temperature control during hyperthermia treatments: theory and simulation," *IEEE Trans. Biomed. Eng.*, vol. 42, no. 8, pp. 818–827, Aug. 1995.

[26] E. Hutchinson, M. Dahleh, and K. Hynynen, "The Feasibility of Mri Feedback Control for Intracavitary Phased Array Hyperthermia Treatments," *InterNatl. J. (Wash.) of Hyperthermia*, vol. 14, no. 1, pp. 39–56, Jan. 1998.

[27] M. Mattingly, R. Roemer, and S. Devasia, "Exact temperature tracking for hyperthermia: a model-based approach," *IEEE Trans. Control Syst. Technol.*, vol. 8, no. 6, pp. 979–992, Nov. 2000.

[28] N. B. Smith, N. K. Merrilees, K. Hynynen, and M. Dahleh, "Control system for an MRI compatible intracavitary ultrasound array for thermal treatment of prostate disease," *InterNatl. J. (Wash.) of Hyperthermia*, vol. 17, no. 3, pp. 271–282, May 2001.

[29] J. K. Enholm, M. O. Kohler, B. Quesson, C. Mougenot, C. T. W. Moonen, and S. D. Sokka, "Improved volumetric mr-hifu ablation by robust binary feedback control," *IEEE Trans. Biomed. Eng.*, vol. 57, no. 1, pp. 103–113, 2010.

[30] J. Palussière, R. Salomir, B. Le Bail, R. Fawaz, B. Quesson, N. Grenier, and C. T. Moonen, "Feasibility of MR-guided focused ultrasound with real-time temperature mapping and continuous sonication for ablation of VX2 carcinoma in rabbit thigh: MR-Guided Focused Ultrasound," *Magn. Reson. Med.*, vol. 49, no. 1, pp. 89–98, Jan. 2003.

[31] C. Mougenot, R. Salomir, J. Palussière, N. Grenier, and C. T. Moonen, "Automatic spatial and temporal temperature control for MR-guided focused ultrasound using fast 3D MR thermometry and multispiral trajectory of the focal point: Automatic Spatial and Temporal Temperature Control," *Magn. Reson. Med.*, vol. 52, no. 5, pp. 1005–1015, Nov. 2004.

[32] M. O. Köhler, C. Mougenot, B. Quesson, J. Enholm, B. Le Bail, C. Laurent, C. T. W. Moonen, and G. J. Ehnholm, "Volumetric HIFU ablation under 3D guidance of rapid MRI thermometry: Volumetric HIFU ablation with 3D rapid MRI thermometry," *Med. Phys.*, vol. 36, no. 8, pp. 3521–3535, July 2009.

[33] J. Enholm, M. Kohler, B. Quesson, C. Mougenot, C. Moonen, and S. Sokka, "Improved Volumetric MR-HIFU Ablation by Robust Binary Feedback Control," *IEEE Trans. Biomed. Eng.*, vol. 57, no. 1, pp. 103–113, Jan. 2010.

[34] D. Arora, M. Skliar, and R. B. Roemer, "Model-predictive control of hyperthermia treatments," *IEEE Trans. Biomed. Eng.*, vol. 49, no. 7, pp. 629–639, 2002.

[35] M. Muddassir, G. Limbert, and D. Navarro-Alarcon, "Development of a numerical multi-layer model of skin subjected to pulsed laser irradiation to optimise thermal stimulation in photorejuvenation procedure," *Comput. Methods Programs Biomed.*, vol. 216, p. 106653, 2022.

[36] H. H. Pennes, "Analysis of tissue and arterial blood temperatures in the resting human forearm," *J. Appl. Physiol.*, vol. 1, no. 2, pp. 93–122, 1948, pMID: 18887578.

[37] X. Li, X. Su, and Y.-H. Liu, "Vision-based robotic manipulation of flexible pcbs," *IEEE ASME Trans. Mechatron.*, vol. 23, no. 6, pp. 2739–2749, 2018.

[38] A. R. Moritz and F. C. Henriques Jr., "Studies of Thermal Injury," *The American J. Pathol.*, pp. 530–549, 1946.

[39] W. G. Connor, E. W. Gerner, R. C. Miller, and M. L. M. Boone, "Prospects for Hyperthermia in Human Cancer Therapy: Part II: Implications of Biological and Physical Data for Applications of Hyperthermia to Man," *Radiology*, vol. 123, no. 2, pp. 497–503, May 1977.

[40] W. C. Dewey, L. E. Hopwood, S. A. Sapareto, and L. E. Gerweck, "Cellular Responses to Combinations of Hyperthermia and Radiation," *Radiology*, vol. 123, no. 2, pp. 463–474, May 1977.

[41] K. J. Henle and L. A. Dethlefsen, "Time-temperature relationships for heat-induced killing of mammalian cells," *Ann. N.Y. Acad. Sci.*, vol. 335, no. 1 Thermal Chara, pp. 234–253, Mar. 1980.
[42] A. Westra and W. Dewey, "Variation in Sensitivity to Heat Shock during the Cell-cycle of Chinese Hamster Cells *in Vitro*," *InterNatl. J. (Wash.) of Radiat. Biol. and Related Studies in Physics, Chemistry and Medicine*, vol. 19, no. 5, pp. 467–477, Jan. 1971.
[43] B. L. Diffey and I. E. Kochevar, "Basic principles of photobiology," in *Photodermatology*, H. W. Lim, H. Hönigsmann, and J. L. M. Hawk, Eds. CRC Press, feb 2007, pp. 29–40.
[44] D. Arora, M. Skliar, D. Cooley, and R. B. Roemer, "Constrained predictive control of thermal therapies for minimum-time delivery of thermal dose," *IEEE Trans. Control Syst. Technol.*, vol. 15, no. 6, pp. 1030–1037, 2007.
[45] H. Kok, P. Wust, P. Stauffer, F. Bardati, G. van Rhoon, and J. Crezee, "Current state of the art of regional hyperthermia treatment planning: a review," *Radiation Oncology*, vol. 10, no. 1, p. 196, Dec. 2015.
[46] D. Arora, M. Skliar, and R. B. Roemer, "Minimum-time thermal dose control of thermal therapies," *IEEE Trans. Biomed. Eng.*, vol. 52, no. 2, pp. 191–200, 2005.
[47] A. Duan, M. Victorova, J. Zhao, Y. Sun, Y. Zheng, and D. Navarro-Alarcon, "Ultrasound-guided assistive robots for scoliosis assessment with optimization-based control and variable impedance," *IEEE Robot. Autom. Lett.*, vol. 7, no. 3, pp. 8106–8113, 2022.
[48] N. Tsuchiya, S. Gibson, T.-C. Tsao, and M. Verhaegen, "Receding-horizon adaptive control of laser beam jitter," *IEEE ASME Trans. Mechatron.*, vol. 21, no. 1, pp. 227–237, 2015.
[49] Y. Li, A. Duan, A. Gratner, and L. Feng, "A geometric programming approach to the optimization of mechatronic systems in early design stages," in *2016 2016 IEEE Int. Conf. Adv. Intell. Mechatron. (AIM)*. IEEE, 2016, pp. 1351–1656.
[50] A. Domahidi, E. Chu, and S. Boyd, "ECOS: An SOCP solver for embedded systems," in *2013 European Control Conference (ECC)*. IEEE, 2013, pp. 3071–3076.
[51] A. Agrawal, R. Verschueren, S. Diamond, and S. Boyd, "A rewriting system for convex optimization problems," *J. Control. Decis.*, vol. 5, no. 1, pp. 42–60, 2018.
[52] A. K. Dabrowska, G. M. Rotaru, S. Derler, F. Spano, M. Camenzind, S. Annaheim, R. Stämpfli, M. Schmid, and R. M. Rossi, "Materials used to simulate physical properties of human skin," *Ski. Res. Technol.*, vol. 22, no. 1, pp. 3–14, 2016.
[53] R. A. Weiss and M. Landthaler, "Lasers and energy sources for skin rejuvenation and epilation," in *Photodermatology*, H. W. Lim, H. Hönigsmann, and J. L. M. Hawk, Eds. CRC Press, 2007, pp. 29–40.
[54] G. Limbert, "Mathematical and computational modelling of skin biophysics: a review," *Proceedings of the Royal Society A: Mathematical, Physical and Eng. Sci.*, vol. 473, no. 2203, p. 20170257, July 2017.
[55] G. Limbert, M. A. Masen, D. Pond, H. K. Graham, M. J. Sherratt, R. Jobanputra, and A. McBride, "Biotribology of the ageing skin—Why we should care," *Biotribology*, vol. 17, pp. 75–90, Mar. 2019.
[56] L. Hu, A. Duan, M. Li, A. Cherubini, L. Li, and D. Navarro-Alarcon, "Paint with the sun: A thermal-vision guided robot to harness solar energy for heliography," *IEEE Sensors Journal*, vol. 22, no. 18, pp. 18 130–18 142, 2022.

Muhammad Muddassir received a master's degree in control science and engineering from Beijing Institute of Technology (BIT), Beijing, China, in 2017, and a PhD in mechanical engineering at The Hong Kong Polytechnic University, Kowloon, Hong Kong, in 2022. His current research interests include the development and control of sensor-guided robotic systems.

Georges Limbert received his master in engineering mechanics (Toulouse, France), a research master in theoretical mechanics (Bordeaux, France), and a Ph.D. in computational biomechanics from the University of Southampton (UK) in 2002.

He is currently an Professor in Mathematical Modelling in Biotribology within the national Centre for Advanced Tribology and Bioengineering Sciences Research Group at the University of Southampton. He is also a Chartered Engineer and Member of the Institution of Mechanical Engineers (IMechE) since 2005 and sits on the board of the Engineering in Medicine and Health Division of the IMechE since 2004. His current research focus is on the biophysical modelling of biological soft tissues and the physics-based modelling of wear of polymers for orthopaedic and tissue engineering applications.

Bin Zhang received his bachelor's degree in detection, guidance and control technology from Beihang University, Beijing, China, in 2017, and his master's degree in control science and engineering from China Academy of Space Technology, Beijing, China, in 2020. Since 2021, he has been pursuing a PhD degree in mechanical engineering at The Hong Kong Polytechnic University, Kowloon, Hong Kong. His current research interests include multi-agent systems and control theory.

Anqing Duan received his Ph.D. degree in robotics from the Italian Institute of Technology and the University of Genoa in 2021. He is currently Research Associate with the Robotics and Machine Intelligence Laboratory at The Hong Kong Polytechnic University. His research interests include medical robotics and learning-based control.

Jun-Jong Tan received the B.Eng. degree in mechanical engineering from The Hong Kong Polytechnic University (PolyU) in 2021. He is currently a Research Assistant with the Laboratory for Artificial Intelligence in Design (AiDLab) of PolyU, Hong Kong. His research interests include the development mechatronic systems, robot control, and image processing.

David Navarro-Alarcon (Senior Member, IEEE) received Ph.D. degree in mechanical and automation engineering from The Chinese University of Hong Kong (CUHK), NT, Hong Kong, in 2014.

From 2014 to 2017, he was a Postdoctoral Fellow and then a Research Assistant Professor with the CUHK T Stone Robotics Institute, Hong Kong. Since 2017, he has been with The Hong Kong Polytechnic University (PolyU), KLN, Kong Kong, where he is currently an Assistant Professor with the Department of Mechanical Engineering, the Principal Investigator of the Robotics and Machine Intelligence Laboratory, and an Associate Investigator at the Research Institute for Smart Ageing. His current research interests include robotics, dynamics, and control theory.